A Low-Complexity Digital Predistortion Technique for Digital I/Q Transmitters

Beikmirza, Mohammadreza; De Vreede, Leo C.N.; Alavi, Morteza S.

DOI
10.1109/IMS37964.2023.10187914

Publication date
2023

Document Version
Final published version

Published in
2023 IEEE/MTT-S International Microwave Symposium, IMS 2023

A Low-Complexity Digital Predistortion Technique For Digital I/Q Transmitters

Mohammadreza Beikmirza, Leo C.N. de Vreede, Morteza S. Alavi
Delft University of Technology, Delft, Netherlands

2023 IEEE/MTT-S International Microwave Symposium - IMS 2023 | 979-8-3503-4764-7/23/$31.00 ©2023 IEEE | DOI: 10.1109/IMS37964.2023.10187914

***Abstract*— This paper presents an advanced yet simple digital pre-distortion (DPD) technique for digital I/Q transmitters (DTXs). Exploiting the I/Q orthogonality, an effective 2×1-D DPD procedure is proposed to bypass the exhaustive 2-D search of the entire constellation diagram. Utilizing this technique, a four-way Doherty DTX is linearized. Measurement results demonstrate that for a non-contiguous six-carrier OFDM-QAM signal with aggregated bandwidth of 150MHz, the ACPR is better than -47.3dBc, and EVM is better than -41/-40dB for channel-1/-6, respectively.**

***Keywords*— Digital pre-distortion, DPD, constellation, mapping, digital transmitter, RF-DAC.**

I. Introduction

Digital transmitters (DTXs) are becoming popular as they supplanted all analog-based TX parts, including digital-to-analog converters, filters, mixers, and power amplifiers (PAs) into one unit of a radio-frequency digital-to-analog converter (RF-DAC) [1], [2]. These DTXs' front end comprises energy-efficient digital PA (DPA) arrays which are driven directly by digital control words that, unlike an analog PA, use digital signals to drive the gates. The output power is controlled by the overall effective width of the activated devices, which varies according to the input amplitude code word (ACW). Unless the switches are scaled nonuniformly [1], the output power is a nonlinear function of the effective switching resistance (R_{On}), causing the ACW-AM nonlinearity. In other words, the ACW-AM nonlinearity is the result of the code-dependent conductance of the drain node [3]–[5]. Moreover, activating the switches and modulating the drain voltage alter the voltage-dependent drain capacitance of the digital power switches. The change in the capacitance, in conjunction with the code-dependent conductance ($1/R_{On}$) of the output stage causes ACW-PM nonlinearity [1], [4]. Typically, as it is conceptually shown in Fig. 1, digital-pre-distortion (DPD) is exploited to confront the DTX nonlinearities, addressing communication standards' stringent in-band linearity and spectral purity requirements verified by error-vector magnitude (EVM) and adjacent channel power ratio (ACLR), respectively.

To tackle these issues, this paper proposes a low-complexity constellation-mapping DPD technique based on 1-D mapping of I/Q baseband signals.

II. The 2×1-D DPD Process

The constellation-mapping DPD is the foundation of the proposed pre-distortion method [6]–[9]. It is based on the

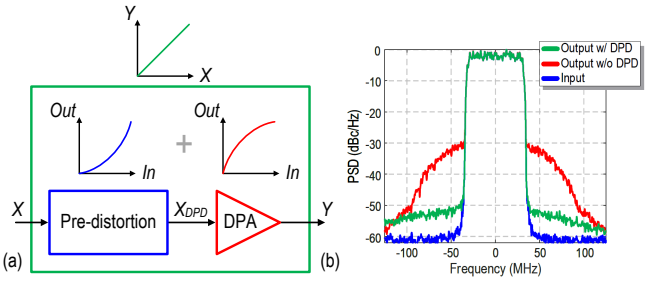

Fig. 1. (a) Basic concept of predistortion, (b) example of the input/output spectrum of a nonlinear PA, with and without DPD.

2×1-D mapping of I and Q baseband data. A complex modulated baseband data can be defined as:

$$\begin{aligned} IQ_{BB_{UP}} &= I_{BB_{UP}} + \mathrm{j} \times Q_{BB_{UP}} \\ &= A_{IQ}\left(I_{BB_{UP}}, Q_{BB_{UP}}\right) \angle \phi_{IQ}\left(I_{BB_{UP}}, Q_{BB_{UP}}\right) \end{aligned} \tag{1}$$

where $I_{BB_{UP}}$ and $Q_{BB_{UP}}$ are shown in Fig. 2(a). Moreover, the envelope and phase information of the associated baseband data are represented by A_{IQ} and ϕ_{IQ}, respectively. The ideal expression for the RF-DAC's modulated RF output is:

$$\begin{aligned} V_{IQ}\left(I_{BB_{UP}}, Q_{BB_{UP}}\right) &= IQ_{BB}\left(I_{BB_{UP}}, Q_{BB_{UP}}\right) \times \exp\left(\mathrm{j}\omega_0 \mathrm{t}\right) \\ &= A_{IQ} \times \exp\left(\mathrm{j}\left(\omega_0 \mathrm{t} + \phi_{IQ}\right)\right) \end{aligned} \tag{2}$$

Nonetheless, since the RF-DAC acts like a nonlinear transmitter, its RF output can be rewritten as:

$$\begin{aligned} &V_{IQ}\left(I_{BB_{UP}}, Q_{BB_{UP}}\right) = \\ &\left(V_I\left(I_{BB_{UP}}, 0\right) + \mathrm{j} \times \mathrm{V}_Q\left(0, Q_{BB_{UP}}\right)\right) \times \exp\left(\mathrm{j}\omega_0 \mathrm{t}\right) \end{aligned} \tag{3}$$

where $V_I\left(I_{BB_{UP}}, 0\right)$ and $V_Q\left(0, Q_{BBUP}\right)$ are the respective nonlinear complex profiles of $I_{BB_{UP}}$ and $Q_{BB_{UP}}$, normalized to their corresponding input codes. These profiles are indicated in Fig. 2(a). In practice, $V_I\left(I_{BB_{UP}}, 0\right)$ and $V_Q\left(0, Q_{BB_{UP}}\right)$ are acquired as follows (Fig. 3): first, due to the orthogonal operation of the I/Q RF-DACs, I_{BB} and Q_{BB} are individually swept and fed to the I/Q DTX. In other words, a ramp function is applied to the I signal while the Q path is zero (Fig. 3(a)). The same process will be used for the Q path in which a ramp function is applied to the Q path while the I path is zero (Fig. 3(b)). In both cases, the subsequent RF output is down-converted, and the related baseband complex signals, i.e., $V_I\left(I_{BB_{UP}}, 0\right)$ and $V_Q\left(0, Q_{BB_{UP}}\right)$, are obtained. Then, the $V_I\left(I_{BB_{UP}}, 0\right)$ and $V_Q\left(0, Q_{BB_{UP}}\right)$ should be rotated such that the maximum I/Q

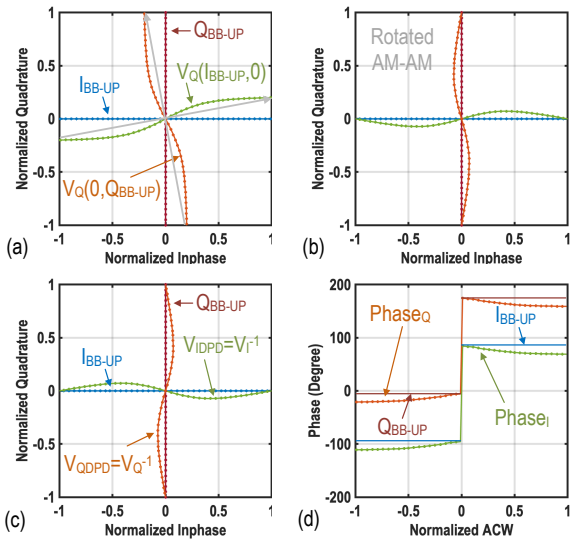

Fig. 2. (a) Input codes along with their corresponding nonlinear output voltages (ACW-AM); (b) phase adjusted nonlinear output voltages; (c) DPD I and Q input code mapping diagram; (d) output phase versus input code (ACW-PM).

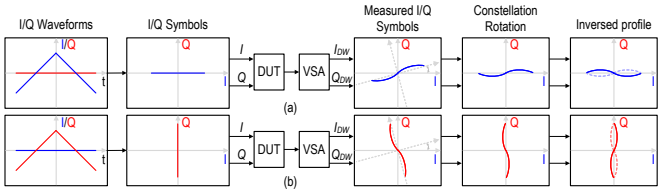

Fig. 3. Practical, $V_I\left(I_{BB_{UP}},0\right)$ and $V_Q\left(0,Q_{BB_{UP}}\right)$ extraction: (a) I path ramp function while the Q path is zero; (b) Q path ramp function while the I path is zero.

code-words and their corresponding point in the measured profiles are aligned (Fig. 2(b)). Next, the inverse function of $V_I\left(I_{BB_{UP}},0\right)$ and $V_Q\left(0,Q_{BB_{UP}}\right)$ are determined as depicted in Fig. 2(c). The following are the I and Q DPD profiles:

$$V_{IDPD}(I,Q)=V_I^{-1}\left(I_{BB_{UP}},0\right)=I_{DPD_I}+\mathrm{j}\times Q_{DPD_I} \tag{4}$$

$$V_{QDPD}(I,Q)=V_Q^{-1}\left(0,Q_{BB_{UP}}\right)=I_{DPD_Q}+\mathrm{j}\times Q_{DPD_Q} \tag{5}$$

Therefore, $I_{BB_{UP}}$ and $Q_{BB_{UP}}$ have the following relations with $V_{IDPD}\left(I,Q\right)$ and $V_{QDPD}\left(I,Q\right)$, respectively:

$$\begin{aligned} I_{BB_{UP}} &= V_I\left(V_I^{-1}\left(I_{BB_{UP}},0\right)\right) \\ &= V_I\left(V_{IDPD}(I,Q)\right)=V_I\left(I_{DPD_I},Q_{DPD_I}\right) \end{aligned} \tag{6}$$

$$\begin{aligned} Q_{BB_{UP}} &= V_Q\left(V_Q^{-1}\left(0,Q_{BB_{UP}}\right)\right) \\ &= V_Q\left(V_{QDPD}(I,Q)\right)=V_Q\left(I_{DPD_Q},Q_{DPD_Q}\right) \end{aligned} \tag{7}$$

Consequently, $I_{BB_{UP}}$ and $Q_{BB_{UP}}$ are independently mapped to $V_{IDPD}\left(I,Q\right)$ and $V_{QDPD}\left(I,Q\right)$, respectively. As a result, this DPD process can be inferred explicitly as a 2×1-D mapping of individual orthogonal $I_{BB_{UP}}$ and $Q_{BB_{UP}}$ signals. Therefore, due to I/Q orthogonality, the DPD does not necessitate a 2-D exhaustive search of the complete

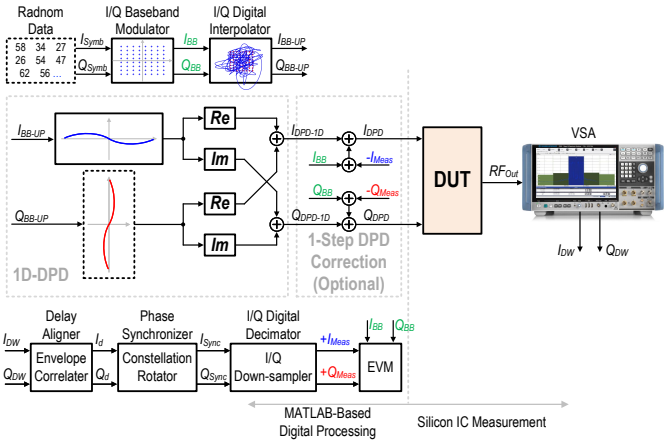

Fig. 4. DPD measurements constellation mapping flow.

constellation diagram as in [10]. Subsequently, I_{DPD} and Q_{DPD} are obtained as follows:

$$I_{DPD}\left(I_{BB_{UP}},Q_{BB_{UP}}\right)=I_{DPD_I}+I_{DPD_Q} \tag{8}$$

$$Q_{DPD}\left(I_{BB_{UP}},Q_{BB_{UP}}\right)=Q_{DPD_I}+Q_{DPD_Q} \tag{9}$$

It should be noted that the ACW-AM and ACW-PM profiles depend on temperature and carrier frequency. Therefore, to account for different frequency/temperature conditions, the relevant DPD profiles must be modified. Moreover, in an energy-efficiency enhanced architectures as in digital Doherty DPAs, transition points where peak branches are activated, will appear as singularities in the ACW-AM and ACW-PM profiles. Thus, to enhance the convergence of the DPD algorithm, the main and peak branches in the ACW-AM and ACW-PM LUTs should be pre-distorted individually.

The constellation mapping measurement setup is exhibited in Fig. 4. The I/Q baseband modulator is fed with I and Q randomly generated symbols (I_{Symb} and Q_{Symb}) in MATLAB to create I_{BB} and Q_{BB} signals. Then, I/Q_{BB} are pulsed-shaped to confine the modulation bandwidth using a square root-raised cosine (SRRC) interpolation filter and up-sampled to the F_S. Afterward, $I_{BB_{UP}}$ and $Q_{BB_{UP}}$ are mapped utilizing the abovementioned technique. Next, the pre-distorted signals (I_{DPD} and Q_{DPD}) are uploaded into designated on-chip SRAMs. A vector signal analyzer (VSA) is then used to down-convert the DTX RF output signal, and the resulting digital in-phase (I_{DW}) and quadrature (Q_{DW}) are then supplied back into MATLAB. Three critical steps should be followed. First, the measurement time delay should be calibrated. Then, the subsequent complex signal phase, i.e., $\phi_{IQ}=\angle\left(I_d+jQ_d\right)$, should be rotated such that the eventual phase, i.e., $\phi_{Sync}=\angle\left(I_{Sync}+jQ_{Sync}\right)$ is the same as the original complex phase, i.e., $\phi_{BB_{UP}}=\angle\left(I_{BB_{UP}}+jQ_{BB_{UP}}\right)$. Finally, I_{Sync} and Q_{Sync} are down-sampled utilizing an SRRC decimation filter to reconstruct the original I/Q baseband modulated signals, i.e., I_{Meas} and Q_{Meas}. The EVM is calculated by comparing the measured I_{Meas} and Q_{Meas} with the original I_{BB} and

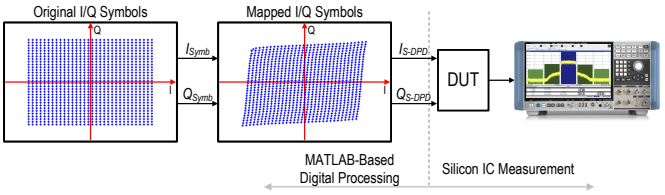

Fig. 5. Mapped I/Q symbols.

Q_{BB}. Using the DPD procedure discussed before, mapped I/Q symbols (I/Q look-up table) are generated, as shown in Fig. 5.

III. Verification of the 2×1-D DPD Process

To verify this method, a 1024-symbol constellation signal is created (Fig. 6(a)). As illustrated in Fig. 6(b), the constellation diagram is continuously snake-likely swept from top-left to top-right and traversed back to its starting point to maintain continuity. The corresponding up-sampled and interpolated $I_{BB_{UP}}$ and $Q_{BB_{UP}}$ trajectories are depicted in Fig. 6(c)-(d). The resulting signals are then pre-distorted (I_{DPD} and Q_{DPD}) and stored in on-chip SRAMs. The effect of the I/Q DPD mapping on the original modulated signals and their corresponding measured trajectories are demonstrated in Fig. 6(e) and Fig. 6(f), respectively. The corresponding I/Q trajectory of the down-converted RF output signal is exhibited in Fig. 6(g), demonstrating an excellent agreement with the original I/Q trajectories of Fig. 6(c). The measured constellation diagram (Fig. 6(h)) is then produced by I_{Sync} and Q_{Sync} after being down-sampled and decimated. Its related EVM is -46.91dB. It should be mentioned that, due to the limited I_{DPD} and Q_{DPD} data length, which are repeatedly fed to the RF-DAC circuit, any discontinuity between the first and last data point creates an undesirable spectral jump. To alleviate this issue and to preserve continuity, the data length of I_{BB} and Q_{BB} are doubled and applied to the SRRC interpolation filter. Subsequently, only half of the data length of the subsequent $I_{BB_{UP}}$ and $Q_{BB_{UP}}$ are exploited and applied to the DPD lookup table. This technique is referred to as a wrap-around process [6]. As a result, the beginning points of the I/Q trajectories of Fig. 6, denoted by circles, have been shaped in such a way as to ensure the continuity of the I/Q signals.

IV. Measurement Results of the 2×1-D DPD Process

The proposed DPD is tested with different signals conforming to the DPD process illustrated in Fig. 4. The I/Q data are generated in MATLAB and then applied to a four-way Doherty DTX [11], [12] which is realized in 40nm bulk CMOS. The output signal is down-converted, digitized using R&S-FSW, and downloaded onto a PC where DPD algorithms are implemented in MATLAB.

First, a multi-carrier signal is generated by combining OFDM, Chirp, M-PSK, and QAM signals (Fig. 7(a)-(e)) with aggregated bandwidth of more than 120MHz at 5.4GHz and

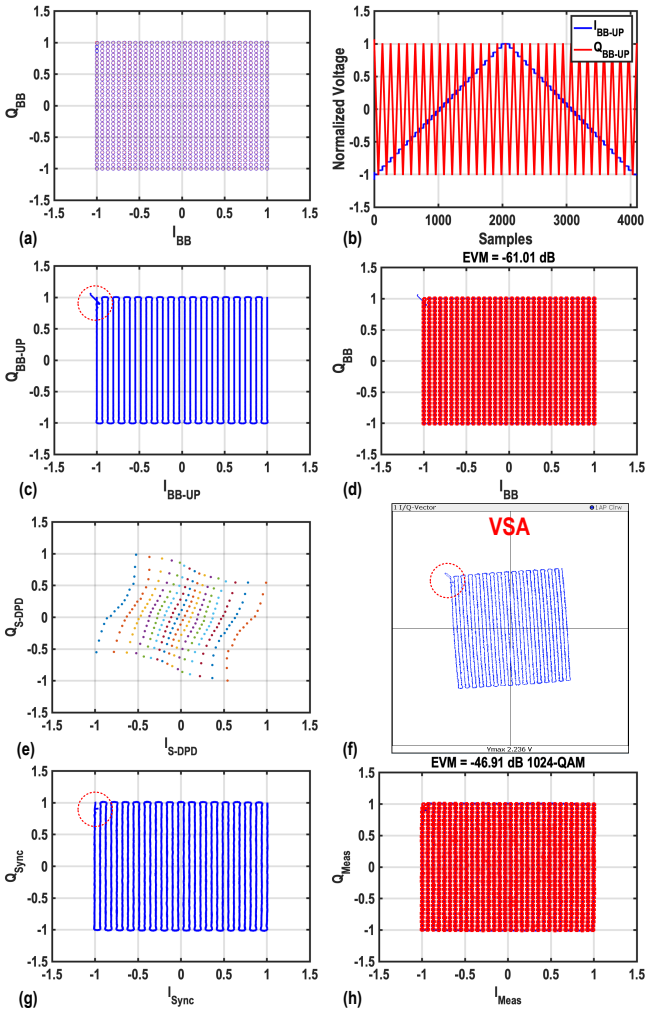

Fig. 6. DPD measurements: (a) 1024-QAM constellation diagram (I_{BB}/Q_{BB}); (b) Trajectories of their related time domain waveforms; (c),(d) $I_{BB_{UP}}/Q_{BB_{UP}}$ trajectories; (e) predistorted I_{DPD}/Q_{DPD} trajectories; (f) measured I_{DW}/Q_{DW} trajectories; (g) measured I_{Sync}/Q_{Sync} trajectories (h) measured 1024-point constellation.

is applied to the DTX and measured at 5.4GHz. Fig. 8(a)-(b) exhibit the measured spectrum of the signal with and without using the DPD. Accordingly, the ACPR is -33.51/-34.10dBc without DPD, while these values are improved to better than -47.33/-48.93dBc, with an alternate channel power ratio of better than -60.04dBc. The constellation diagrams are depicted in Fig. 8(c)-(f). The measured EVM is -44.32dB, -35.83dB, -31.43dB, and -41.83dB for 64-QAM-OFDM, Chirp, M-PSK, and 64-QAM channels, respectively. Moreover, the average power is 19.36dBm, while its related drain efficiency is 40%.

Second, the DTX is tested with six-carrier×10MHz QAM and OFDM signals with aggregated bandwidth of more than 150MHz at 5.4GHz. Fig. 9(a)-(b) show the measured spectrum of the signal with and without application of the DPD. The ACPR is improved from -33.57dBc to better than -47.34dBc, while the constellation diagrams depicted in Fig. 9(c)-(d) present an EVM of -41.03/-40.01dB

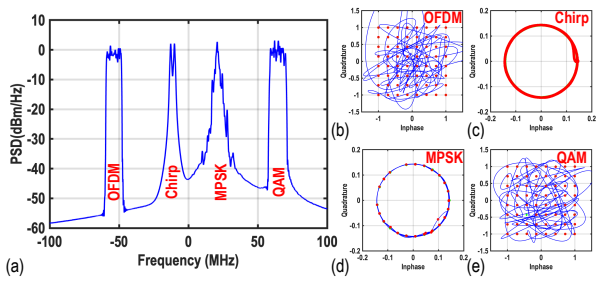

Fig. 7. (a) Generated multi-channel OFDM, Chirp, M-PSK, and QAM signal spectrum; (b)-(e) corresponding constellation diagrams.

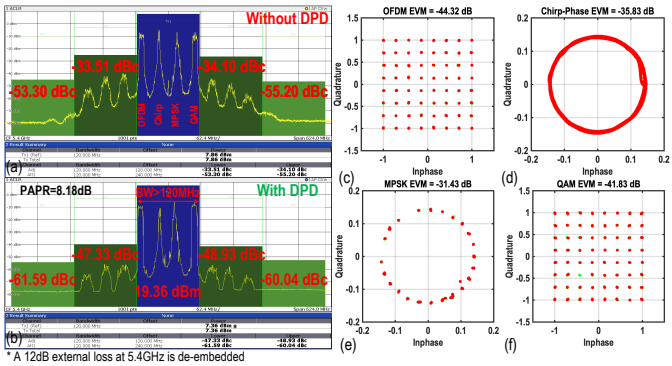

Fig. 8. Multi-channel OFDM, Chirp, M-PSK, and QAM signal measurement results, (a) spectrum without DPD, (b) spectrum with DPD, (c)-(d) corresponding constellation diagrams with DPD.

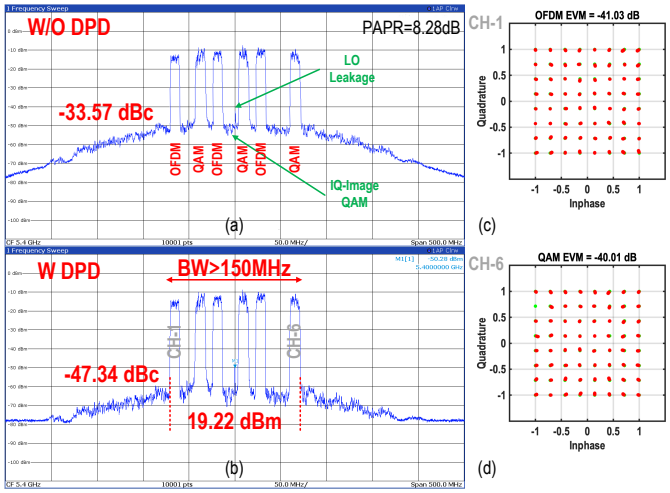

Fig. 9. Multi-channel signal OFDM and QAM measurement results, (a)-(b) spectrum with and without DPD; (c)-(d) channel-l/-6 constellation diagrams.

for channel-1/-6, respectively. The four-way Doherty DTX achieves an average output power of more than 19dBm while maintaining the average drain and system efficiency of more than 40% and 24%, respectively.

V. Conclusion and Discussion

This paper presents a low-complexity 2×1-D constellation-mapping-based DPD technique for the I/Q DTXs. Specifically, this DPD process can be inferred as a 2×1-D mapping of individual orthogonal I/Q signals. The 2×1-D LUT is created using a snake-like 1024-QAM modulation. It is demonstrated that by using this technique, for a four-carrier OFDM+Chirp+M-PSK+QAM signal with aggregated bandwidth of 120MHz, the ACPR is better than 47.3dBc. The EVMs are -44.32dB, -35.83dB, -31.43dB, and -41.83dB, respectively, while generating more than 19dBm power with better than 40% drain efficiency. To the best of the author's knowledge, it is the first reported measurement with the mentioned signal configuration.

It is worth mentioning that the I/Q combination method has a significant impact on the I/Q interaction. In an analog domain combination method, the possible overlap between the I/Q signals causes unwanted I/Q interaction, degrading the EVM and linearity. Therefore, a DPD may experience some difficulties with compression when both I/Q are active and at their maximum code-word. However, in a more digitally-intensive realization, the I/Q combination can also be carried out in the digital domain, addressing the challenges of analog-intensive I/Q RF signals summation, yielding a more effective DPD process. Moreover, although the memory effects in a well-designed DPA are typically less severe than in an analog PA since only the bias connection of the final stage tends to contribute to these memory effects, future work may include memory effects in the proposed DPD process.

References

[1] M. Hashemi *et al.*, "An Intrinsically Linear Wideband Polar Digital Power Amplifier," *IEEE Journal of Solid-State Circuits*, vol. 52, no. 12, pp. 3312–3328, dec 2017.

[2] M. Beikmirza *et al.*, "A Wideband Energy-Efficient Multi-Mode CMOS Digital Transmitter," *IEEE Journal of Solid-State Circuits*, vol. 58, no. 3, pp. 677–690, 2023.

[3] S. Zheng and H. C. Luong, "A cmos wcdma/wlan digital polar transmitter with am replica feedback linearization," *IEEE Journal of Solid-State Circuits*, vol. 48, no. 7, pp. 1701–1709, 2013.

[4] M. Alavi, J. Mehta, and R. Staszewski, *Radio-Frequency Digital-to-Analog Converters: Implementation in Nanoscale CMOS*. Elsevier Science, 2016.

[5] M. Mehrpoo *et al.*, "A Wideband Linear I/Q-Interleaving DDRM," *IEEE Journal of Solid-State Circuits*, vol. 53, no. 5, pp. 1361–1373, may 2018.

[6] M. S. Alavi *et al.*, "A Wideband $2\times$ 13-bit All-Digital I/Q RF-DAC," *IEEE Transactions on Microwave Theory and Techniques*, vol. 62, no. 4, pp. 732–752, apr 2014.

[7] V. Petrovic, "Reduction of spurious emission from radio transmitters. by means of modulation feedback," in *Proc. IEE Conf. on Radio. Spectrum Conservation Techniques, Sept. 1983*, 1983, pp. 44–49.

[8] G. Karam and H. Sari, "A data predistortion technique with memory for qam radio systems," *IEEE Transactions on Communications*, vol. 39, no. 2, pp. 336–344, 1991.

[9] J. H. Qureshi *et al.*, "A 90-w peak power gan outphasing amplifier with optimum input signal conditioning," *IEEE Transactions on Microwave Theory and Techniques*, vol. 57, no. 8, pp. 1925–1935, 2009.

[10] C. Lu *et al.*, "A 24.7dBm All-Digital RF Transmitter For Multimode Broadband Applications in 40nm CMOS," in *2013 IEEE International Solid-State Circuits Conference Digest of Technical Papers*, 2013, pp. 332–333.

[11] M. Beikmirza *et al.*, "6.2 A 4-Way Doherty Digital Transmitter Featuring 50%-LO Signed IQ Interleave Upconversion with more than 27dBm Peak Power and 40% Drain Efficiency at 10dB Power Back-Off Operating in the 5GHz Band," in *Digest of Technical Papers - IEEE International Solid-State Circuits Conference*, vol. 64, feb 2021, pp. 92–94.

[12] M. Beikmirza *et al.*, "A Wideband Four-Way Doherty Bits-In RF-Out CMOS Transmitter," *IEEE Journal of Solid-State Circuits*, vol. 56, no. 12, pp. 3768–3783, 2021.